technologies

MDPI

*Article*

# Steam Distillation of Citrus Waste Extract for Antimicrobial Metal Nanoparticle Synthesis

**Javier Emanuel Castañeda-Aude [1,2,3], Enrique Díaz Barriga-Castro [4], Lizbeth Liliana Díaz-Muñoz [1], Javier Alberto Garza-Cervantes [1,3], José Rodríguez-Mirasol [2], José Rubén Morones-Ramírez [1,3], Héctor Javier Amézquita-García [1,3], David Alejandro De Haro-Del Río [5], Angel León-Buitimea [5], Noe Macias-Segura [6] and Carlos Enrique Escárcega-González [1,*]**

1 Facultad de Ciencias Químicas, Universidad Autónoma de Nuevo León, Pedro de alba, s/n, San Nicolás de los Garza 66455, Nuevo León, Mexico; javier.castanedaau@uanl.edu.mx (J.E.C.-A.); lizbeth_liliana_3@hotmail.com (L.L.D.-M.); javier.garzacn@uanl.edu.mx (J.A.G.-C.); jose.moronesrmr@uanl.edu.mx (J.R.M.-R.); hector.amezquitagr@uanl.edu.mx (H.J.A.-G.)
2 Departamento de Ingeniería Química, Universidad de Málaga, Andalucia Tech, Campus de Teatinos s/n, 29010 Málaga, Spain; mirasol@uma.es
3 Facultad de Ciencias Químicas, Universidad Autónoma de Nuevo León, Centro de Investigación en Biotecnología y Nanotecnología, Parque de Investigación e Innovación Tecnológica, Apodaca 66629, Nuevo León, Mexico
4 Centro de Investigación de Química Aplicada, Enrique Reyna H. No. 140, San José de los Cerritos, Saltillo 25294, Coahuila, Mexico; enrique.diazbarriga@ciqa.edu.mx
5 Escuela de Ingeniería y Ciencias, Tecnológico de Monterrey, Ave. Eugenio Garza Sada 2501, Monterrey 64849, Nuevo León, Mexico; deharo@tec.mx (D.A.D.H.-D.R.); angel.lbuitimea@tec.mx (A.L.-B.)
6 Departamento de Inmunología, Facultad de Medicina, Universidad Autónoma de Nuevo León, Monterrey 64460, Nuevo León, Mexico; noe.maciass@uanl.edu.mx
* Correspondence: carlos.escarcegagzz@uanl.edu.mx

## Abstract

This research presents a novel, sustainable, and eco-friendly method for the rapid green synthesis of nanoparticles with antibacterial properties. This method employs steam distillation to extract reducing and stabilizing agents from orange peel waste, followed by ultrasound-assisted synthesis. To the best of our knowledge, this is the first reported integration of these two techniques for nanoparticle production. The extracted materials were then subjected to rigorous characterization through a combination of analytical techniques, including FTIR, HPLC, and TEM. These analytical approaches enabled a comprehensive analysis of the synthesized NPs, revealing their size distribution within the range of 1.5 to 14 nm. Among the synthesized nanomaterials, AgNPs exhibited the most potent antibacterial activity, with statistically significant minimum inhibitory concentrations (MICs) of 16 ppm for *E. coli* ATCC and 32 ppm for resistant *E. coli* and *E. faecalis* strains. This study underscored the promise of valorizing citrus waste for nanomaterial synthesis and introduced a novel, scalable methodology for producing bioactive nanoparticles, promoting a more sustainable technology for this purpose. Notably, this research aligns with United Nations Sustainable Development Goal 12, which promotes responsible consumption and production by transforming organic waste into high-value functional nanomaterials for biomedical and environmental applications.

**Keywords:** orange peel; antimicrobial nanoparticles; sustainable nanotechnology

check for updates

Academic Editor: Nam-Trung Nguyen

Received: 30 May 2025
Revised: 6 July 2025
Accepted: 9 July 2025
Published: 14 July 2025

**Citation:** Castañeda-Aude, J.E.; Díaz Barriga-Castro, E.; Díaz-Muñoz, L.L.; Garza-Cervantes, J.A.; Rodríguez-Mirasol, J.; Morones-Ramírez, J.R.; Amézquita-García, H.J.; De Haro-Del Río, D.A.; León-Buitimea, A.; Macias-Segura, N.; et al. Steam Distillation of Citrus Waste Extract for Antimicrobial Metal Nanoparticle Synthesis. *Technologies* **2025**, *13*, 303. https://doi.org/10.3390/technologies13070303

**Copyright:** © 2025 by the authors. Licensee MDPI, Basel, Switzerland. This article is an open access article distributed under the terms and conditions of the Creative Commons Attribution (CC BY) license (https://creativecommons.org/licenses/by/4.0/).

## 1. Introduction

Due to the increase in population, the food industry has had to significantly grow year after year to meet the global demand for food [1]. This growth has simultaneously increased the generation of byproducts and waste, contributing significantly to environmental pollution on a global scale [2]. Improper management of organic waste from the production, preparation, and consumption of fruits and vegetables, when disposed of in landfills, can have a negative impact on the environment as these waste materials generate leachates, contaminating the soil, groundwater, and even the air [3–6]. Therefore, in recent years, various methods have been explored to repurpose this waste and produce high-value products, with the goal of minimizing the amount of material that goes unused [7,8]. This approach directly supports the United Nations Sustainable Development Goal 12, which encourages responsible consumption and production patterns by promoting the valorization of waste materials into useful products rather than contributing to environmental pollution. Additionally, these new products can be used in other areas of interest such as water treatment, dye and drug removal, catalyst synthesis, biomedical, electronics, and environmental applications [9–11]. This promotes a circular economy and helps address existing problems.

In this context, citrus fruits are among the most consumed and popular fruits worldwide. According to the Food and Agriculture Organization of the United Nations (FAO), approximately 143 million tons of citrus fruits were produced in 2021, with oranges accounting for 48% of that sum [12]. Oranges offer significant nutritional benefits as they contain various bioactive compounds, such as phenolic compounds, flavonoids, vitamins, and minerals [13]. These compounds help reduce the risk of combat diseases such as cancer, cardiovascular diseases, osteoarthritis, anti-atherosclerotic effects, and platelet anti-aggregation, among others [14,15]. Despite their nutritional advantages, oranges also generate a high amount of waste, with 50–60% of their weight being waste, primarily consisting of peels, membranes, and seeds. Of this waste percentage, 60–75% is solely from the peel [16,17]. This waste is of particular interest due to the large quantities generated annually. Like the fruit itself, it contains a significant number of valuable bioactive compounds such as phenolic acids, polyphenols, flavonoids, vitamins, carotenoids, amines, pectin, and minerals that are often discarded [18,19], which can be used to obtain different by-products due to their antioxidant activity with antimicrobial, antifungal, antiviral, and anticancer properties [20].

In recent years, various techniques have been employed to find the most effective way to extract these bioactive components with antioxidant activity from orange peels, including maceration, agitation, steam distillation, ultrasound-assisted extraction, and the use of different solvents [21–23]. Steam distillation offers a notable advantage in extracting bioactive compounds from orange peels due to its simplified assembly. The system allows for rapid cleaning and replacement of the column after extraction, eliminating the need for additional filtration treatments. This efficiency not only saves time but also improves the purity of the extracted compounds, making steam distillation a candidate to harness the bioactive potential of orange peel [24].

Given this situation, researchers are particularly interested in using these antioxidants for nanomaterial synthesis. Specifically, they can facilitate the formation of metallic nanoparticles (NPs) by reducing metal ions and acting as stabilizing agents [25]. The aromatic hydroxyl groups in these antioxidant compounds facilitate the formation of metallic nanoparticles by donating electrons during oxidation, thereby reducing the metal salts [26]. For example, silver nanoparticles have been synthesized using extracts from the peels of *Citrus limon*, *Citrus tangerina*, and *Citrus sinensis*; these NPs have a size of 5–80 nm and exhibit antibacterial properties against *Escherichia coli* and *Staphylococcus aureus* with

inhibition zones of 7 to 21 mm [27]. Additionally, iron oxide NPs, derived from extracts of *Citrus sinensis* peels, have been synthesized, exhibiting antibacterial properties against *Escherichia coli* and *Micrococcus*. These NPs displayed inhibition zones of 12.6 nm and 11.3 nm, respectively [28]. Zinc oxide NPs obtained from *Citrus sinensis* peel extract have also been utilized as coatings for strawberries, exhibiting a remarkable anti-fungal effect against *Botrytis cinerea*, inhibiting its growth by more than 94%. Additionally, these NPs exhibited antimicrobial properties, with a MIC of 20 mg/L against *Staphylococcus aureus* and 40 mg/L against *Escherichia coli* [29]. On the other hand, orange peel extract has been used to synthesize selenium NPs with sizes ranging from 16 to 95 nm, exhibiting antimicrobial properties against *S. aureus* ATCC 29213, as well as multidrug-resistant bacteria such as *Pseudomonas aeruginosa*, *Escherichia coli*, and *Klebsiella pneumoniae* [30].

Previous research has explored the antibacterial mechanisms of metal nanoparticles (MNPs), though the exact process remains unclear. Several steps have been proposed to explain their activity. Initially, MNPs interact with the bacterial cell wall, which shows an affinity for the carboxyl groups present in the wall. Once MNPs are absorbed by the cell wall, they generate reactive oxygen species (ROS) [31]. The resulting ROS production ultimately leads to the disruption and destruction of the bacterial membrane [32].

It has been proposed that silver nanoparticles (AgNPs) adhere to bacterial cell walls through electrostatic interactions between $Ag^+$ ions and functional groups such as carboxyl, amino, and phosphate groups present in the cell membrane [33]. This interaction can disrupt the membrane's structural integrity, potentially enabling the nanoparticles to penetrate the cell. As a result, the proton motive force is compromised, leading to pH imbalances and the release of additional $Ag^+$ ions. These ions can further damage the cell by disrupting membrane function or inducing DNA damage [34,35]. Under this context, CuNPs are particularly effective against gram-positive bacteria, as these bacteria have significant amounts of carboxyl and amino groups in their cell walls [36,37]. In addition, the oxidative stress generated by the CuNPs causes cellular damage to the bacteria [38]. The mechanisms of action of FeNPs and ZnONPs exhibit similarities to those observed for AgNPs and CuNPs. The antibacterial effects of FeNPs primarily result from the generation of ROS, which causes oxidative damage to bacterial cells [39]. Similarly, ZnONPs disrupt bacterial cell membranes, leading to the production of ROS and the release of zinc ions. These zinc ions contribute to antibacterial activity by damaging DNA and interacting with biomolecules such as proteins and lipids, thereby compromising cellular integrity and function [40].

To synthesize these NPs, researchers have studied different routes to obtain nanomaterials with desirable characteristics [41]. Methods such as laser ablation, mechanical milling, physical and chemical vapor deposition, and green methods have been employed for this purpose [42–45]. Green techniques are considered as an available route due to the high availability of agro-industrial waste that can be used for the synthesis of NPs, in addition to being techniques that employ environmentally friendly synthesis conditions [46]. Therefore, the objective of this study is to develop and evaluate a novel green synthesis method for nanoparticles by extracting bioactive compounds from orange peel waste through steam distillation, followed by nanoparticle formation assisted by an ultrasound bath. This innovative combination of extraction and synthesis techniques applied for the first time in this context aims to produce AgNPs, CuNPs, $Fe_2O_3$NPs, and ZnONPs under environmentally friendly and reproducible conditions. Furthermore, the antibacterial activity of the resulting NPs will be assessed against *Escherichia coli* ATCC 11229, resistant *Escherichia coli*, and resistant *Enterococcus faecalis* strains.

## 2. Materials and Methods

### *2.1. Sample Collection*

Fresh oranges (*Citrus sinensis*) were collected from August to October in Nuevo León, Mexico. These oranges were thoroughly washed with distilled water and peeled before being processed in a food mill (Waring WSG60, Waring Products, Torrington, CT, USA) at 25,000 rpm for 60 s to achieve a uniform particle size. Subsequently, 20 g of processed oranges were weighed for use in the extraction of reducing and stabilizing agents.

### *2.2. Steam Distillation Apparatus and Procedure of Bioactive Compounds Extraction from Citrus Peels*

The steam generation process involves a stirring heating plate, and an Erlenmeyer flask connected via hoses to a polyethylene column (Figure 1). The condenser is maintained at a temperature of 5 °C to ensure rapid and complete condensation of the vapor, which is rich in polyphenols and flavonoids [24]. Notably, the system is designed for easy cleaning after each extraction process. Additionally, the polyethylene column offers the flexibility of quick and simple replacement, allowing for scalability with longer columns.

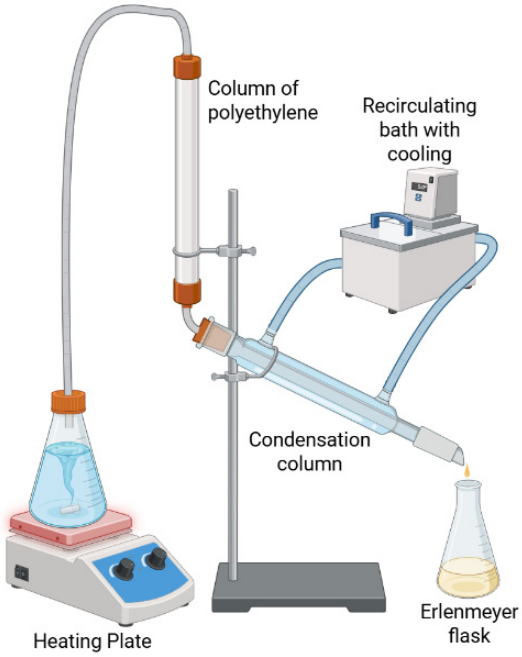



**Figure 1.** Steam distillation apparatus for extracting polyphenols and flavonoids from orange peel.

The polyethylene column was filled with 20 g of crushed orange peel, and filter paper was placed at the outlet to prevent particle carryover. Steam passes through the sample, carrying polyphenols and flavonoids to the condenser and the collection beaker. The process is halted upon obtaining 100 mL of extract, which is then stored at 4 °C for subsequent use [47].

### *2.3. Preparation of Nanoparticles*

First, 20 mL of the metallic salt solution ($AgNO_3$, $Cu(NO_3)_2$, $Fe(NO_3)_3$, or $Zn(NO_3)_2$) with a concentration of 0.1 M was placed in a 50 mL Corning tube. Subsequently, 20 mL of orange peel extract was added to the tube. The tube was then placed in an ultrasonic bath (Branson 2510R-MTH, Branson Ultrasonics, Brookfield, CT, USA) and allowed to react at room temperature for 60 min. During this period, the formation of metallic NPs was observed through a color change in the mixture. The formation of AgNPs and $Fe_2O_3$NPs was indicated by a change in color from amber to coffee-black; for CuNPs, the color change was from blue to dark green, and for ZnONPs, it shifted from amber to pale amber. After

this reaction time, once the synthesis was complete, the NPs were separated from the mixture using centrifugation with a Centra CL2 machine, adjusted to 4000 rpm for 15 min. The separated NPs were then filtered, and the remaining residue was washed twice with 96% ethanol to eliminate any impurities and organic material. Finally, this process resulted in stable AgNPs, CuNPs, $Fe_2O_3$NPs, and ZnONPs.

### 2.4. Characterization of Orange Peel Extract

The extract was analyzed using Fourier Transform Infrared Spectroscopy (FTIR), which was utilized with the Spectrum One apparatus from Perkin Elmer to capture infrared spectra with a scan of 4000 to 600 $cm^{-1}$. This technique was used to identify the functional groups present in the extract and in the orange peel before and after extraction.

For the determination of flavonoids in orange peel extract, the sample was prepared by diluting the extract to 5% ($v/v$) with deionized water. The solution was then filtered through a 0.45 µm membrane filter (Millipore, Burlington, MA, USA) prior to HPLC analysis. Chromatographic separation was performed using an Agilent 1260 Infinity II HPLC (Agilent Technologies, Santa Clara, CA, USA) system equipped with a C18 reversed-phase column (InfinityLab Poroshell 120 EC-C18, 4.6 × 150 mm, 4 µm; Agilent Technologies, Santa Clara, CA, USA) maintained at 37 °C. A gradient elution was employed using phase A (water with 0.5% acetic acid) and phase B (acetonitrile) as the mobile phases. Gradients of the following phases were used: 10–30% B over 15.9 min, 35% B at 19.8 min and maintained at 35% B for 4 min with an operation time of 40 min at a flow rate of 1 mL/min, the injection rate was 15.87 microliters, and the UV detection wavelength was 280 nm. For the identification of flavonoids, standards for naringin (Sigma-Aldrich, St. Louis, MO, USA) and hesperidin (Sigma-Aldrich) were injected at concentrations of 250 ppm.

### 2.5. Characterization of Nanoparticles

The NPs obtained underwent a range of analyses to discern their microstructural attributes. UV-visible spectrophotometry was employed to examine them using a Genesys 10S (Thermo Fisher Scientific, Waltham, MA, USA) machine with wavelengths 200–1000 nm. Fourier Transform Infrared Spectroscopy was utilized with the Spectrum One apparatus (PerkinElmer Inc., Waltham, MA, USA) to capture infrared spectra with a scan of 4000 to 600 $cm^{-1}$. To analyze their structural and morphological features, transmission electron microscopy (TEM) was employed using a FEI-TITAN 80–300 kV microscope (FEI Company, Hillsboro, OR, USA) operated at 300 kV. The samples were studied using several transmission techniques, including conventional TEM, selected area electron diffraction (SAED), high-resolution transmission electron microscopy (HRTEM), and energy-dispersive X-ray spectroscopy (EDS) for elemental chemical analysis.

### 2.6. Tested Bacteria

The bacteria used in the antimicrobial trials were *Escherichia coli* ATCC 11229, multi-resistant *Enterococcus faecalis* (resistant to ampicillin, ciprofloxacin, levofloxacin, and high-level gentamicin), and multi-resistant *Escherichia coli* (resistant to cephalexin, ceftriaxone, cefotaxime, cefuroxime, ampicillin/sulbactam, and trimethoprim/sulfamethoxazole).

### 2.7. Antimicrobial Activity of NPs

MIC assays were conducted in 96-well plates. The typical serial microdilution procedure was followed [48,49]. Initially, NPs stock solutions were prepared in LB medium at a concentration of 1024 ppm. A total of 200 µL of these NPs stocks was then added to the 96-well plate. Serial dilutions of NPs were performed by transferring 100 µL from the current well to the next, containing 100 µL of culture medium, and discarding the final

100 µL from the last dilution. The tested NPs concentrations ranged from 512 to 0.5 ppm once the bacterial inoculum was added.

For inoculation, a 100 µL aliquot of an overnight bacterial culture (incubated at 37 °C, 150 rpm) was transferred to a fresh LB tube and further incubated at 37 °C until an optical density at 600 nm ($OD_{600}$) equivalent to $10^7$ cells/mL was reached (approximately 0.12 absorbance using the Multiskan GO instrument; Thermo Fisher Scientific, Waltham, MA, USA. After reaching the desired $OD_{600}$, a 1:100 dilution was made in fresh LB medium, and 100 µL of this diluted culture was inoculated into each well, resulting in a final bacterial concentration of approximately 105 cells/mL per well.

Subsequently, 100 µL of the bacterial suspension was added to each well, and the 96-well plate was incubated at 37 °C and 150 rpm. Optical density readings at 600 nm were taken after 24 h. All assays were performed in triplicate, including appropriate growth and sterility controls. The data were analyzed to determine the percentage of bacterial growth and inhibition at the specified NP concentrations.

To determine statistically significant differences between treatments (i.e., varying nanoparticle concentrations) and the control group, antimicrobial activity data were analyzed using one-way analysis of variance (ANOVA), followed by Tukey's post hoc test for multiple comparisons. Each nanoparticle type and bacterial strain was evaluated independently to ensure the accurate assessment of treatment effects. A significant level of $p < 0.05$ was employed to identify meaningful differences between groups. Statistical analyses were performed using Microsoft Excel with the Real Statistics Add-in. The results obtained are reported as the mean ± standard deviation from three independent experiments ($n = 3$).

## 3. Results and Discussion

### *3.1. Characterization of Extract and NPs*

As demonstrated in Figure 2, the chromatographic analysis of the orange peel extract obtained through steam distillation using Agilent 1260 Infinity II HPLC revealed the presence of hesperidin at a retention time of 12.4 min. This result is consistent with the findings of previous studies of flavonoid extraction from orange peel [50,51]. However, this extraction methodology did not effectively isolate naringin. The chromatogram further reveals the presence of other flavonoids, as evidenced by the multiple minor peaks detected. Of note is the prominent and intense peak of hesperidin, which signifies its predominant concentration within the extraction matrix.

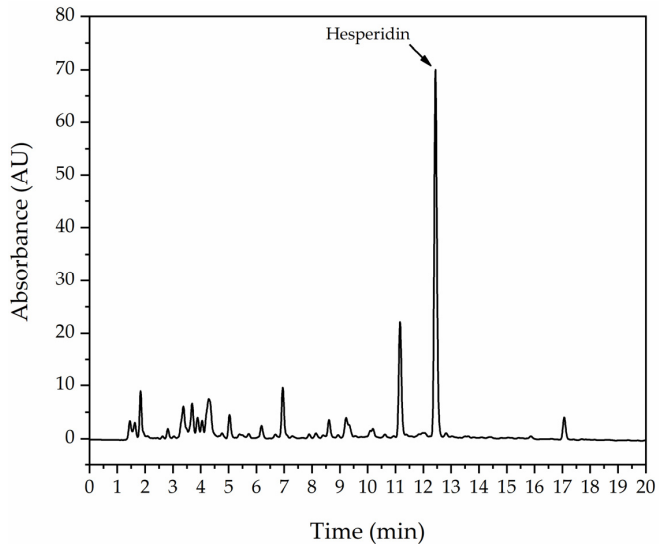



**Figure 2.** HPLC chromatogram at 280 nm of orange peel extract showing hesperidin detection.

In this study, the UV-Vis spectrum was used as the first method to confirm the synthesis of NPs using the orange peel extract. Figure 3 shows the UV-Vis absorption spectra of all the metallic NPs. The blue spectra confirm the presence of AgNPs produced using an aqueous solution containing orange peel extracts [52]. These AgNPs exhibit a plasmon resonance spectrum with a maximum absorption peak at 448 nm. For the CuNPs (Figure 3 in red), a slight peak is observed at 306 nm. Although these values are outside the typical range, they suggest the possible synthesis of CuNPs, indicating that they may have an extremely small particle size, explaining the deviation in the spectrum [53]. Similarly, the green spectra show a peak at 286 nm, which corresponds to the $Fe_2O_3$NPs, located close to the characteristic range of 300–400 nm for these types of NPs, successfully confirming their synthesis [54]. In the yellow spectra, it can be observed that the ZnONPs are located at 282 nm, which can be attributed to the formation of ZnONPs 300–375 nm [55].

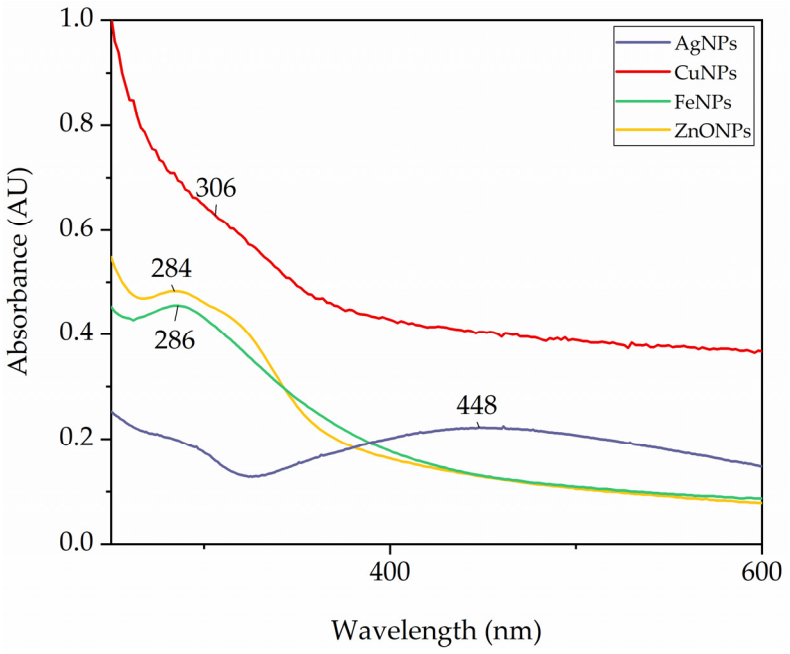



**Figure 3.** UV-Vis absorption spectra of metal nanoparticles synthesized with orange peel extracts.

The FTIR spectra of the orange peel extract obtained through steam distillation, as well as the orange peel before and after extraction, were examined to gain insight into their chemical composition and functional groups. Figure 4a displays the FTIR spectrum of the orange peel extract obtained through steam distillation, revealing a peak at 1057 $cm^{-1}$ attributed to the stretching vibrations of the C-O bonds [56]. Additionally, a peak located at 1646 $cm^{-1}$ corresponds to the vibrations of the C=O bonds of the carbonyl groups [57]. The distinctive band at 3327 $cm^{-1}$ is a result of the large number of hydroxyl groups present [58]. A comparison between the orange peel before and after extraction (Figure 4b,c) and after extraction (Figure 4c) revealed significant changes. Although several bands observed in the pre-extraction orange peel spectrum persisted after extraction, there was a decrease in the intensity of certain bands, notably at 2926 $cm^{-1}$, which corresponds to the C-H stretching vibration [59]. The decrease in this band suggests that alkyl groups were effectively transferred to the extract, which is supported by the presence of the same band in the extract (Figure 4a). This suggests that carbonyl-containing compounds, such as fatty acids or esters, were partially transferred from the peel to the extract during steam distillation, as evidenced by the presence of the 1646 $cm^{-1}$ band in both the extract (Figure 4a) and the peel after extraction (Figure 4c) [60].

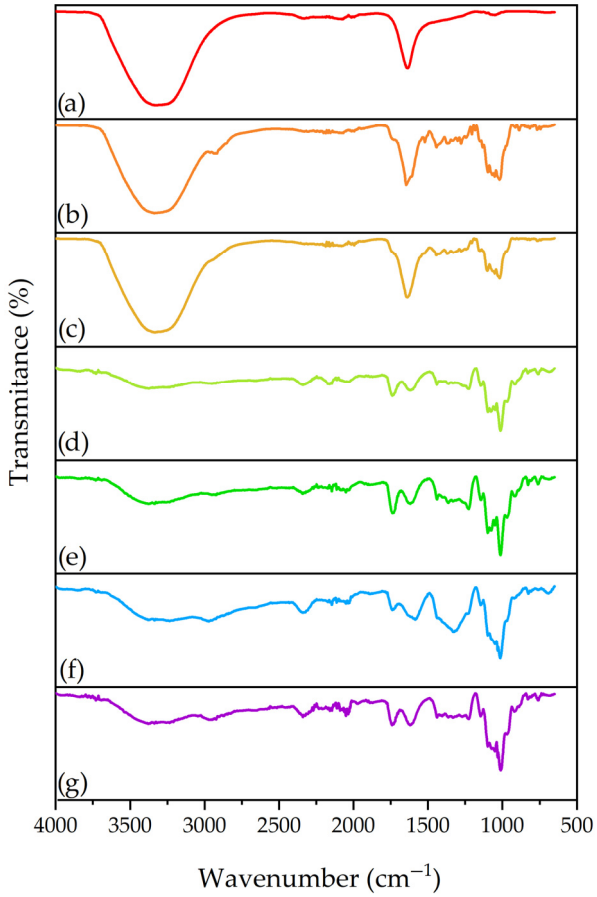



**Figure 4.** FTIR spectrum of (**a**) Orange peel extract obtained by steam distillation, (**b**) Orange peel before extraction, (**c**) Orange peel after extraction, (**d**) AgNPs synthesized, (**e**) CuNPs synthesized, (**f**) $Fe_2O_3$NPs synthesized and (**g**) ZnONPs synthesized.

This comparative analysis not only demonstrates the efficiency of the steam distillation process in transferring bioactive compounds from the peel (Figure 4b) to the extract (Figure 4a) but also allows for the correlation of the functional groups present (hydroxyl, carbonyl, and C-H) with their role in nanoparticle synthesis. The presence of hydroxyl groups in the extract (Figure 4a) suggests their active role as reducing and stabilizing agents, while the decrease in bands associated with alkyl groups in the peel after extraction (Figure 4c) confirms their mobilization into the liquid phase. Thus, FTIR analysis of the peel and extract provides a complete picture of the extraction process and offers an understanding of the surface chemistry of the synthesized NPs.

The FTIR spectra of NPs are shown in Figure 4d–g. These spectra were analyzed to investigate the chemical composition and presence of functional groups. It is evident that the synthesized and analyzed NPs exhibit bands and peaks because there are functional groups that stabilize and cover the NPs [61]. For example, the formation of metallic NPs is expected to produce characteristic M-O vibrations around ~560 cm$^{-1}$, which can be masked by overlapping with signals from organic bands [27]. The observed peaks at 763 and 831 cm$^{-1}$ correspond to the out-of-plane bending vibrations of C -H, which are associated with essential oils found in orange peel, such as limonene [62]. Additionally, the peaks at 1014 and 1101 cm$^{-1}$ correspond to the stretching vibrations of C-O bonds which can be attributed to flavonoids present such as hesperidin, naringin, or linalool compounds [63], while the peak at 1443 cm$^{-1}$ is associated with the bending vibrations of C-H bonds related to the deformation vibration of methyl and methylene groups [64], indicating the presence of proteins [63], indicating that these compounds remained on the NPs surface, while the

at 1627 $cm^{-1}$ that may correspond to the C=O stretching vibrations in amides or C=C stretching in conjugated alkenes or aromatics [65]. This peak at 1737 $cm^{-1}$ is characteristic of the stretching vibration of the carbonyl group (C=O) in esters or carboxylic acids. The peaks in the range of 1840 to 2290 $cm^{-1}$ are a result of $CO_2$ present in the environment [66], and the peak at 2963 $cm^{-1}$ is associated with the C-H stretching vibration of methyl or methylene groups in organic compounds. Finally, the band between 3106 and 3648 $cm^{-1}$ corresponds to the stretching vibrations of the O-H and N-H bonds, respectively, suggesting the presence of alcohol and phenol groups within the extract [67]. These findings reinforce the hypothesis of a phenolic-based stabilizing layer [68].

These results suggest that bioactive compounds in the extract obtained by water vapor not only act as reducing agents during synthesis but also function as stabilizing agents, forming an organic layer around the nanoparticles that prevents agglomeration and enhances their colloidal stability (Figure 4d–g). In this context, FTIR complements structural (TEM, SAED) and optical (UV–Vis) analyses by providing a more complete view of the interaction between phenolic and flavonoid compounds from the citrus waste matrix and the metal surface and elucidates the migration of specific functional groups onto the nanoparticles.

Microstructural analysis was performed using TEM techniques (HRTEM and SAED). These techniques were used to analyze the size and shape of nanoparticles. Additionally, histogram data were analyzed to ascertain the size distribution of them. Despite being synthesized using the same orange peel extract, each type of metal nanoparticle exhibited unique sizes and morphologies. In Figures 5a, 6a, 7a and 8a, the TEM micrographs reveal the morphology of the NPs, which exhibit a quasi-spherical shape with various sizes ranging from 1.5 to 14 nm.

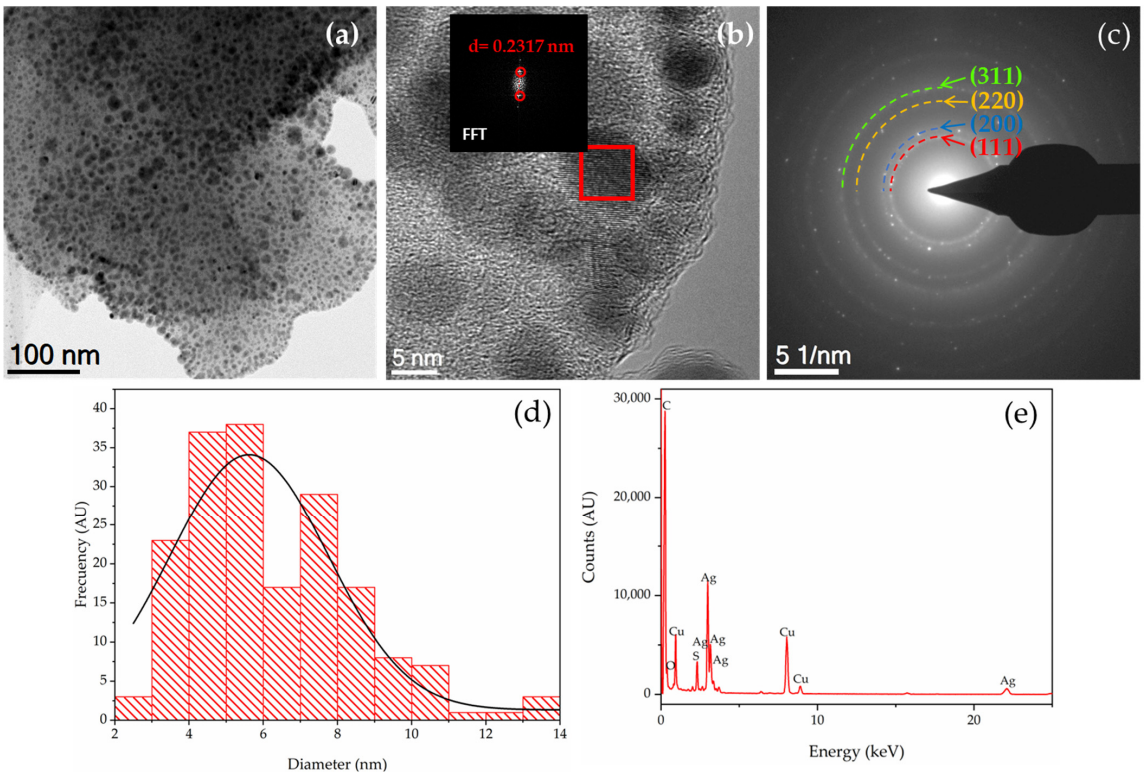



**Figure 5.** Characterization of the AgNPs synthesized with orange peel extract obtained by steam distillation. (**a**) TEM micrograph, (**b**) High-resolution TEM micrograph, the inset shows the FFT part of the corresponding section, (**c**) SAED pattern with the rings labeled, (**d**) Histogram showing the particle size distribution, (**e**) EDS spectrum with the peaks labeled.

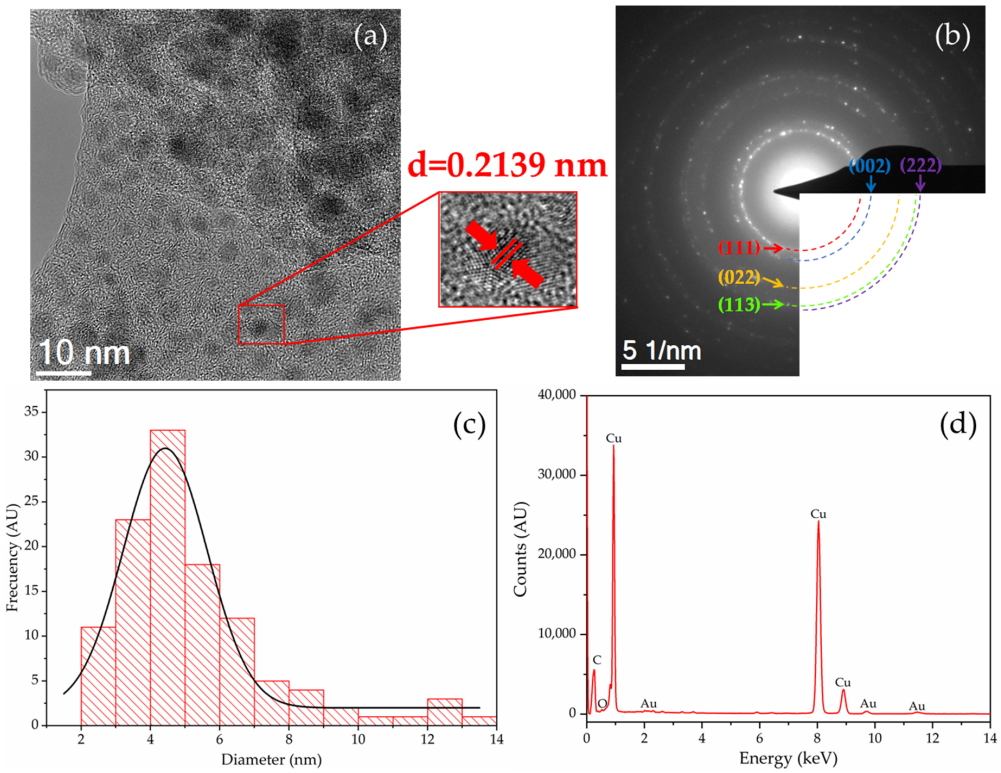



**Figure 6.** Characterization of the CuNPs synthesized with orange peel extract obtained by steam distillation. (**a**) High-resolution TEM micrograph: the inset shows an increase in the interplanar distance of the corresponding section. (**b**) SAED pattern of the CuNPs with the rings labeled. (**c**) Histogram showing the particle size distribution. (**d**) EDS spectrum of the CuNPs with the peaks labeled.

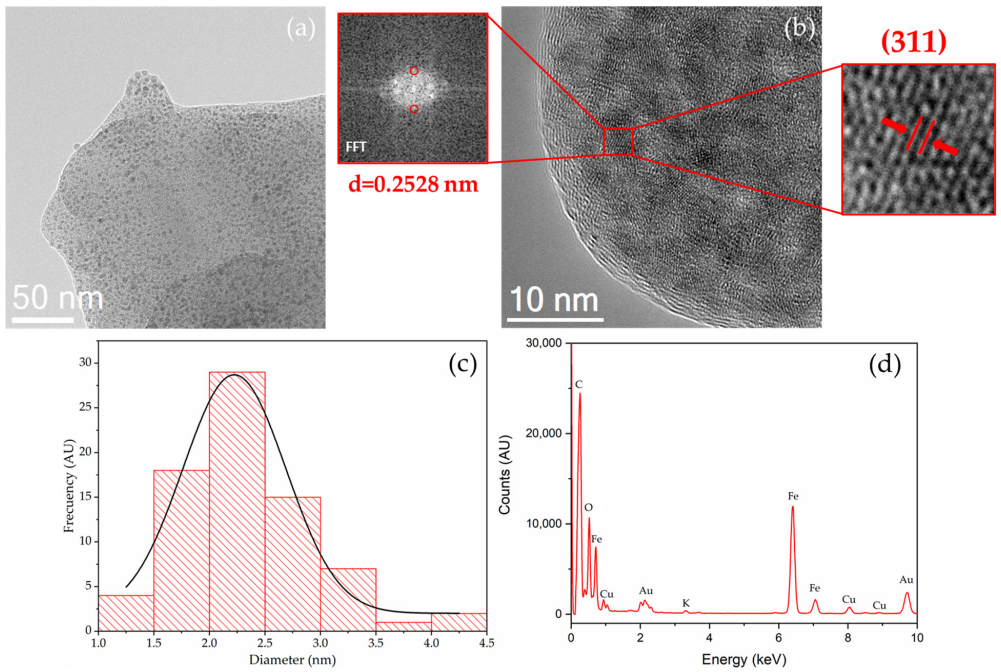



**Figure 7.** Characterization of the $Fe_2O_3$NPs synthesized with orange peel extract obtained by steam distillation. (**a**) TEM micrograph. (**b**) HRTEM micrograph: the inset shows the FFT part and the interplanar distance of the corresponding section. (**c**) Histogram showing the particle size distribution. (**d**) EDS spectrum with the peaks labeled.

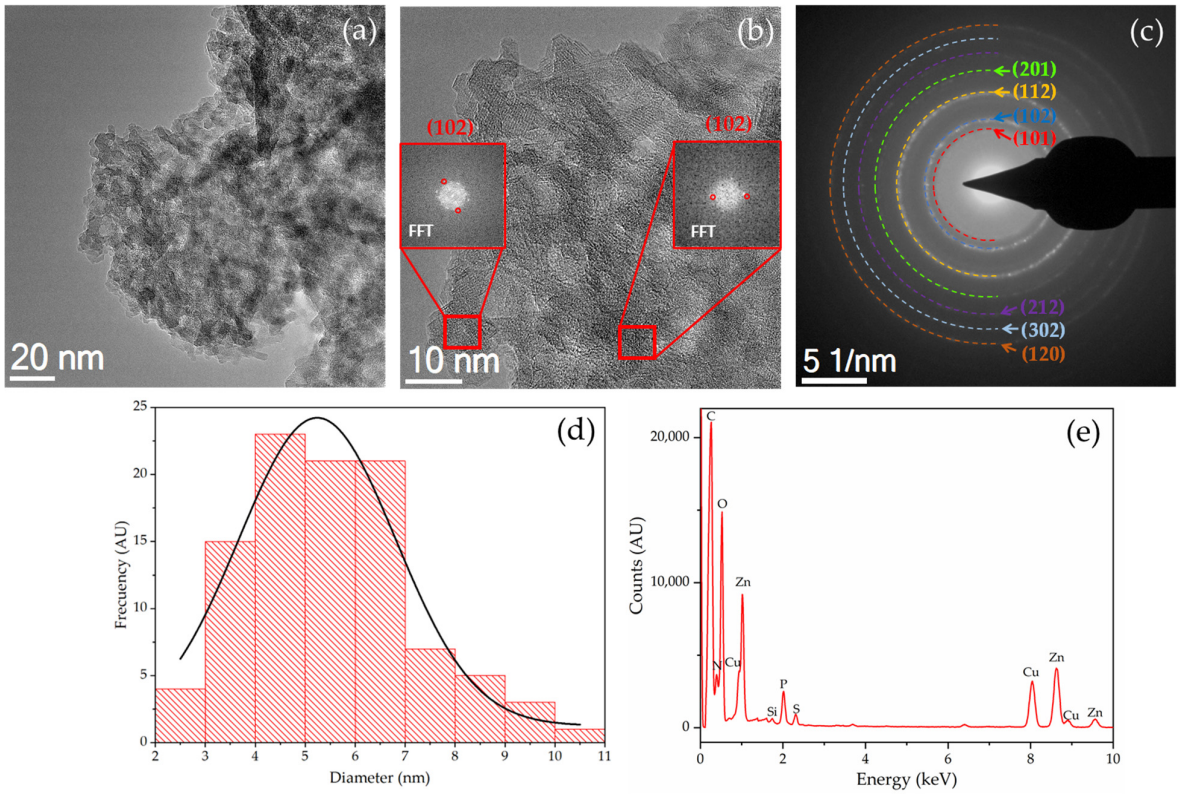



**Figure 8.** Characterization of the ZnONPs synthesized with orange peel extract obtained by steam distillation. (**a**) TEM micrograph. (**b**) High-resolution TEM micrograph: the insets show the FFT part of the corresponding section. (**c**) SAED pattern with the rings labeled. (**d**) Histogram showing the particle size distribution. (**e**) EDS spectrum with the peaks labeled.

Figure 5a shows AgNPs dispersed within and surrounded by organic residues from the orange peel extract. On the other hand, Figure 5b shows a typical HRTEM micrograph of the NPs, where it is possible to see the crystalline planes coinciding whit the metallic silver structure in the (111) direction with an interplanar distance of 0.2317 nm, this can be confirmed by the Joint Committee on Powder Diffraction Standards (JCPDS) number 87-0720. Figure 5c shows a representative SAED diffraction pattern of the nanoparticles synthesized from orange extract. In this pattern, well-defined rings are clearly observed, which are attributed to the (111), (200), (220), and (311) crystalline planes of the face-centered cubic (fcc) metallic silver, as confirmed by JCPDS file number 87-0720. Figure 5d shows the size distribution of AgNPs, which can be described by a log-normal distribution with a value of 5.6 nm and a standard deviation of 0.33 nm. Elemental analysis of the chemical composition was performed by EDS (Figure 5e indicates that the main component of the sample is Ag. In addition, C and traces of O were detected. The C peak could come mainly from the lacey-carbon film and the organic material product of the synthesis.

As illustrated in Figure 6a, it is observed that the CuNPs are coated with organic material from the orange peel, furthermore, a close-up of the crystalline planes of the CuNPs was performed where an interplanar distance of 0.2139 nm was obtained which coincides with the (111) plane of the metallic copper structure, as confirmed by JCPDS number 85-1326. On the other hand, the SAED ring analysis depicted in Figure 6b revealed that the CuNPs have the (111), (200), (220), (311), (222), (311), (420), and (422) crystalline planes, attributing to the crystalline planes of metallic copper, in line with JCPDS 85-1326 reference. The size distribution of CuNPs, as depicted in Figure 6c, shows that with the use of orange peel extract, CuNPs have an average size of 4.3 nm and a standard deviation of 0.09 nm. Figure 6d shows the EDS analysis for CuNPs, in which different elements were

detected, mainly the peaks corresponding to copper, as well as traces of O, confirming the presence of metallic copper. In addition, C was detected coming from the residual organic material or from the lacey-carbon film, as well as Au coming from the same grid. The spectrum in general indicated a high level of purity, as no other elements were detected.

Figure 7a shows that $Fe_2O_3$ nanoparticles can be observed dispersed on the residual organic material of the synthesis. On the other hand, in Figure 7b, an HRTEM micrograph of these nanoparticles can be observed, in which the crystalline planes belonging to $Fe_2O_3$ can be observed in the (311) direction. The FFT image confirms that this crystalline plane has an interplanar distance of 0.2528 nm; this is confirmed by the JCPDS file number 39-1346. Figure 7c shows the size distribution of the $Fe_2O_3$NPs with an average size of 2.2 nm and a standard deviation of 0.03 nm. In addition, the elemental analysis is depicted in Figure 7d, confirming the presence of Fe and O, elements belonging to the $Fe_2O_3$ nanoparticles. The C and Cu peaks are mainly attributed to the lacey-carbon film.

Figure 8a shows that the morphology of the ZnONPs has agglomerated into a larger structure, indicating growth of the ZnO crystals. The FFTs shown in Figure 8b correspond to the zinc oxide structure with crystalline planes in the (102) direction. These planes are supported by JCPDS file number 96-101-1260. At the same time, the SAED ring analysis depicted in Figure 8c confirms crystalline planes in the (101), (102), (112), (201), (212), (302), and (220) directions belonging to ZnO, as confirmed by JCPDS 96-101-1260. Figure 8d depicts the size distribution profile of the ZnONPs, which ranged from 2 to 11 nm, exhibiting a mean particle size of 5.2 nm and a standard deviation of 0.15 nm. Finally, the EDS spectrum of the synthesised ZnO nanoparticles (Figure 8e) shows the characteristic peak of zinc at 8.63 keV and oxygen at 0.52 keV, components essential for the formation of ZnO. Notably, the EDS analysis also revealed the presence of copper, carbon originating from the carbon lacey films in the copper TEM grid.

This study is consistent with existing literature on the use of plant and fruit extracts for generating ultrasmall NPs, reinforcing the effectiveness of such methods. Specifically, $Fe_2O_3$NPs synthesized via our approach averaged 2.2 nm, while AgNPs, CuNPs and ZnONPs measured 5.6, 4.4 and 5.2 nm, respectively. Our method, which employs orange peel extract obtained using steam distillation, produced NPs comparable in size to those reported in previous studies. For instance, AgNPs of 1.70 nm were synthesized using glycerol as a reducer and polyvinylpyrrolidone as a stabilizer [69]; the *Cymbopogon citratus* extract yielded CuNPs of 2.90 nm [70]; and Cupressus sempervirens extract produced NPs with an average size of 1.5 nm [71].

Moreover, EDS and SAED analyses of AgNPs synthesized using *Tagetes erecta* extracts [72], CuNPs from *S. cervicorne* algae [73], $Fe_3O_4$NPs from Moringa oleifera extracts [74], and ZnONPs from pumpkin seeds [75] have yielded similar results, further validating the reliability of these green synthesis approaches.

It has been reported that polyphenolic compounds such as flavonoids have the ability to reduce $Cu^{2+}$ ions to their metallic form ($Cu^0$) by releasing reactive hydrogen atoms during tautomeric shifts from the enol to the keto form [76]. Notably, the orange peel extract used in this study contains flavonoids capable of facilitating this reduction mechanism. Once $Cu^0$ is formed, nucleation occurs, during which the $Cu^0$ nuclei aggregate to form copper nanoparticles (CuNPs). These CuNPs are subsequently chelated by flavonoids through functional groups such as hydroxyl and carbonyl groups, which stabilize the CuNPs in their metallic form [76]. In contrast, consistent with polyol-type chemistry, the reducing agents in the extract are not strong enough to reduce $Fe^{3+}$ or $Zn^{2+}$ to their metallic states. Instead, the reaction favors the formation of $Fe(OH)_3$ and $Zn(OH)_2$ intermediates, which can dehydrate over time to form $Fe_2O_3$ and ZnO nanoparticles (oxide NPs obtained in this study), respectively, in agreement with polyol-mediated syntheses [77].

However, our study distinguishes itself by employing steam-distilled orange peel extract as an efficient, clean, and scalable method. Beyond ensuring reproducibility, this approach enhances environmental sustainability by repurposing agroindustrial waste, offering a greener and more practical alternative for NPs synthesis.

### *3.2. Antimicrobial Activity*

The antibacterial efficacy of NPs synthesized using orange peel extract was evaluated against both Gram-negative (*E. coli* ATCC and a resistant strain) and Gram-positive (*E. faecalis* resistant) bacteria by determining their MICs through a serial dilution method (Figure 9). Among the tested nanoparticles, AgNPs exhibited the most pronounced inhibitory effect, with complete growth inhibition observed at concentrations $\geq$ 32 ppm for all three bacterial strains. Conversely, CuNPs, $Fe_2O_3$NPs, and ZnONPs exhibited no discernible growth inhibition at most concentrations, although some reductions were visually apparent at higher doses.

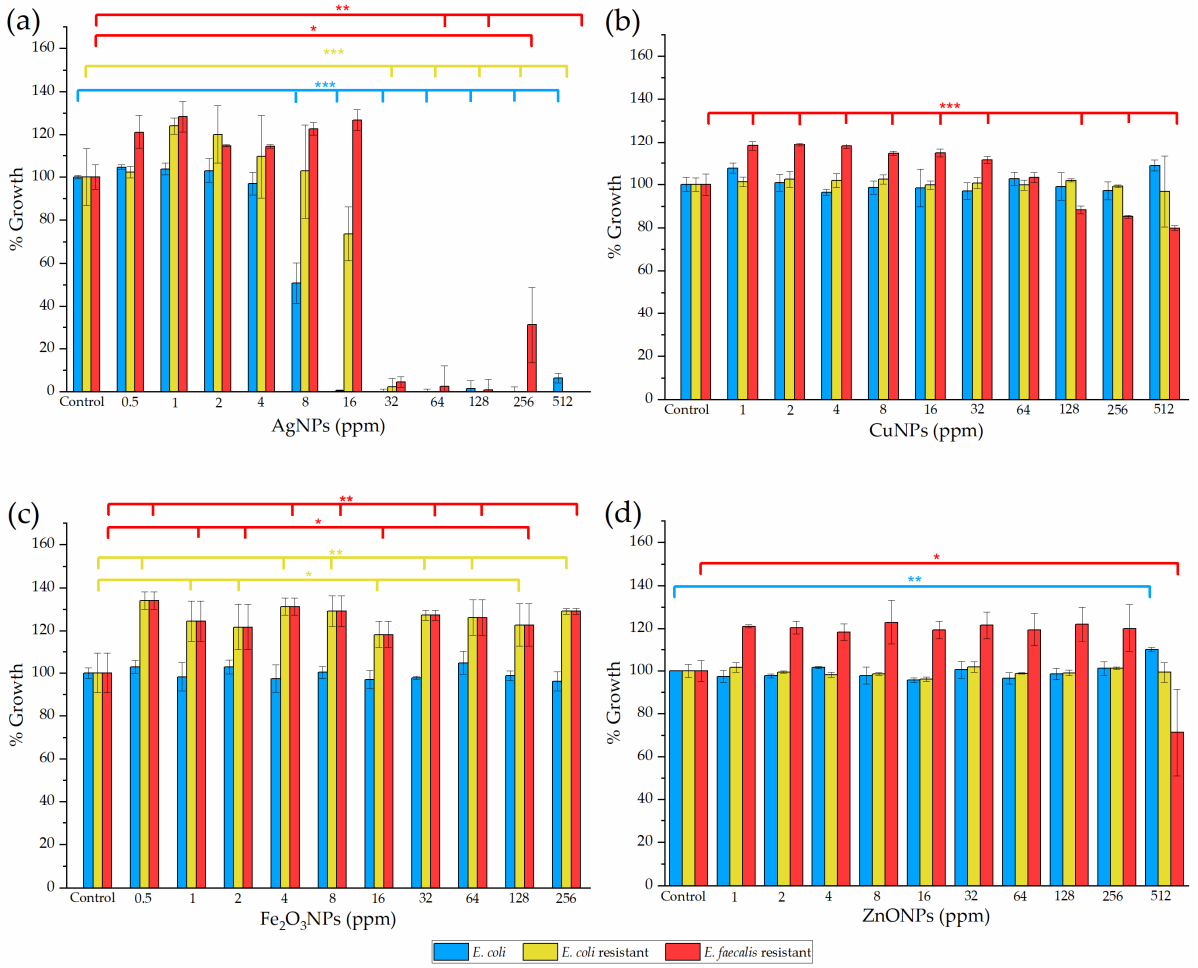



**Figure 9.** Effect on bacterial growth of *Escherichia coli* ATCC, resistant *Escherichia coli* strain and resistant *Enterococcus faecalis* exposed to: (**a**) AgNPs, (**b**) CuNPs, (**c**) $Fe_2O_3$NPs and (**d**) ZnONPs. Error bars represent the standard deviation of experiments performed in triplicate ($n$ = 3). Statistical significance was determined by one-way ANOVA followed by Tukey's post hoc test (* $p < 0.05$, ** $p < 0.01$, *** $p < 0.001$).

As illustrated in Figure 9a, the inhibitory effect of AgNPs on bacterial growth is concentration dependent. At low concentrations (0.5 to 4 ppm), bacterial growth remains relatively high across all strains. However, at concentrations greater than 8 ppm, a marked decrease in bacterial growth is evident, particularly in the *E. coli* ATCC strain. Statistically

significant differences ($p < 0.01$) compared with the control were confirmed for *E. coli* ATCC across the 8 to 512 ppm range. For the resistant *E. coli* strain, significant inhibition ($p < 0.01$) was observed from 32 to 512 ppm. In the case of *E. faecalis* resistant, growth inhibition became significant at 64, 128, and 512 ppm ($p < 0.01$) and at 256 ppm ($p < 0.05$). These findings substantiate the marked and extensive antibacterial efficacy of AgNPs, particularly against *E. coli*, with *E. faecalis* exhibiting a less pronounced yet statistically substantiated response at elevated concentrations.

Conversely, as demonstrated in Figure 9b, CuNPs exhibited no statistically significant antibacterial effect against *E. coli* ATCC or the resistant *E. coli* strain at any of the concentrations evaluated. However, the resistant *E. faecalis* strain exhibited statistically significant growth inhibition ($p < 0.01$) at all concentrations from 1 to 512 ppm, except for 64 ppm, where no significant difference was observed. While the magnitude of inhibition was modest overall, the results suggest a specific susceptibility of *E. faecalis* to CuNPs, with the Gram-negative strains remaining largely unaffected under the tested conditions.

As shown in Figure 9c, $Fe_2O_3$NPs did not produce a statistically significant inhibition of *E. coli* ATCC at any of the tested concentrations. In contrast, both resistant *E. coli* and resistant *E. faecalis* strains exhibited statistically significant growth inhibition at several concentrations. Specifically, strong inhibition ($p < 0.01$) was observed at 0.5, 4, 8, 32, 64, and 256 ppm, while moderate inhibition ($p < 0.05$) occurred at 1, 2, 16, and 128 ppm. Despite these effects, the overall response was not strongly dose dependent, and the magnitude of inhibition remained moderate. These findings suggest that $Fe_2O_3$NPs possess selective antibacterial activity against resistant strains, though with variable consistency.

Figure 9d indicates that ZnONPs exhibited limited antibacterial activity overall. Statistically significant inhibition was observed only at the highest concentration tested (512 ppm). *E. coli* ATCC exhibited a significant reduction in growth at $p < 0.01$, and resistant *E. faecalis* exhibited a significant reduction at $p < 0.05$. No significant effects were detected for the resistant *E. coli* strain at any concentration. The findings imply that ZnONPs possess limited antibacterial potential under the experimental conditions, exhibiting only modest effectiveness at elevated concentrations and in specific bacterial strains.

The MIC values obtained for NPs synthesized from orange peel extract are presented in Table 1. Table 2 presents the results from the literature, enabling a comparison between the MICs obtained in this study and those reported for the same NPs and bacterial strains synthesized via different green methods. The findings of this study indicate that AgNPs synthesized in this work exhibit strong and broad-spectrum inhibitory capacity against both resistant and non-resistant bacterial strains, with statistically significant effects ($p < 0.01$) observed across a wide range of concentrations. In contrast, CuNPs, $Fe_2O_3$NPs, and ZnONPs required higher concentrations to produce measurable inhibition, and their efficacy was more selective and strain dependent. Specifically, CuNPs exhibited a statistically significant effect ($p < 0.01$) only against *E. faecalis* resistant across most concentrations, while ZnONPs and $Fe_2O_3$NPs demonstrated significant effects primarily against resistant strains at select concentrations, as confirmed using one-way ANOVA followed by Tukey's test.

**Table 1.** MIC values of NPs for the three bacterial strains evaluated in this study.

| Bacteria | MICs (ppm) | | | |
|---|---|---|---|---|
| | AgNPs | CuNPs | $Fe_2O_3$NPs | ZnONPs |
| *E. coli* ATCC-11229 | 16 | >512 | >512 | >512 |
| *E. coli* resistant | 32 | >512 | >512 | >512 |
| *E. faecalis* resistant | 32 | >512 | >512 | >512 |

**Table 2.** MIC values of NPs for the bacterial strains tested from different sources.

| Bacteria | Treatment | MIC (ppm) | Extract | Reference |
|---|---|---|---|---|
| *E. coli* | AgNPs | 12.50 | *Syngonium podophyllum* | [78] |
| *E. coli* | AgNPs | 1250 | *Mimusops elengi* | [79] |
| *E. coli* | AgNPs | 50 | *Pimpinella anisum* L. | [80] |
| *E. faecalis* (OU510, ATCC29212, SL92, SL96, SL86) | AgNPs | 250 | *Moringa oleifera* L. | [81] |
| *E. coli* | CuNPs | 8000 | *Falcaria vulgaris* | [82] |
| *E. coli*<br>*E. faecalis* | CuNPs | 288<br>31.3 | Ascorbic acid | [83] |
| *E. coli*<br>*E. faecalis* | FeNPs | 12.5<br>7.4 | *T. indica* | [84] |
| *E. coli* ATCC 25922 | FeNPs | 50 | *A. haussknechtii* | [85] |
| *E. faecalis* | ZnONPs | 1250 | *Punica granatum* | [86] |
| *E. coli*<br>*E. faecalis* | ZnONPs | 3.9 | *Curcuma longa* | [87] |

These findings underscore the importance of complementing apparent inhibitory trends with statistical validation, as some treatments, despite visible reductions in bacterial growth, did not consistently reach statistical significance. A comparison of the results with data reported in the literature reveals that NPs synthesized from various biological sources require concentrations ranging from 3 to 8000 ppm. The results obtained here position AgNPs as the most effective antimicrobial agent among those tested. Nevertheless, further evaluation with optimized dosing, extended exposure times, or additional biological endpoints is recommended to confirm and extend the observed effects of CuNPs, $Fe_2O_3$NPs, and ZnONPs.

An innovative element of this study is the extraction method employed, which represents a significant advance beyond the antimicrobial performance of the synthesized NPs. Conventional extraction techniques, including organic solvent extraction, maceration, and Soxhlet processes, have been superseded by steam distillation. This novel method offers a more efficient, expeditious, and eco-friendly approach for recovering bioactive compounds from citrus waste. This methodology aligns with the 12 principles of green chemistry, as it reduces solvent consumption, shortens extraction time, simplifies purification steps, and improves reproducibility, making it especially attractive for green synthesis applications. Furthermore, its scalability and compatibility with waste recovery systems enhance its suitability for the sustainable production of nanomaterials. This study is pioneering in its application of steam-distilled orange peel extract, assisted by ultrasound, for the synthesis of metal nanoparticles. The antimicrobial activity of this process has been validated.

## 4. Conclusions

This study demonstrated that the steam distillation of orange peel, in conjunction with ultrasound-assisted synthesis, offers an innovative and sustainable approach for obtaining extracts with reducing and stabilizing properties. These extracts are well suited for the green synthesis of metal nanoparticles with validated antibacterial activity. This approach combines eco-compatibility, operational simplicity, and cost-effectiveness, presenting a scalable alternative for the development of functional nanomaterials. The antimicrobial evaluation revealed that AgNPs exhibited the most potent and broad-spectrum activity, with statistically significant MIC values across all tested bacterial strains, including resistant *E. coli* and *E. faecalis* at concentrations as low as 16 to 32 ppm. In contrast, CuNPs, $Fe_2O_3$NPs, and ZnONPs demonstrated more selective or limited antimicrobial effects.

CuNPs exhibited significant inhibition only against *E. faecalis* resistant, while $Fe_2O_3$NPs and ZnONPs exhibited strain-specific responses at higher concentrations. These findings indicate that, while AgNPs emerge as the most promising candidates for antimicrobial applications, further optimization is warranted for the other NPs, particularly through dose adjustment, combination therapies, or application in alternative biological contexts such as fungal inhibition, biofilm control, or environmental remediation.

This study emphasizes the valorization of citrus waste as a more sustainable technology and environmentally friendly approach for the green synthesis of nanomaterials, contributing directly to Sustainable Development Goal 12. By applying principles of green chemistry and circular economy, citrus peels are repurposed as a renewable resource for the eco-friendly production of metallic and/or metal oxide nanoparticles. In addition to promoting waste reduction and resource efficiency, this method also yields functional nanomaterials with promising antimicrobial properties, thus demonstrating both environmental and biomedical benefits.

**Author Contributions:** Conceptualization, J.R.M.-R., J.R.-M. and C.E.E.-G.; methodology, J.A.G.-C. and N.M.-S.; validation, J.R.-M., D.A.D.H.-D.R., A.L.-B. and H.J.A.-G.; Formal analysis, J.E.C.-A.; investigation, J.E.C.-A.; resources, C.E.E.-G.; data curation, E.D.B.-C.; writing—original draft preparation, J.E.C.-A.; writing—review and editing, E.D.B.-C., L.L.D.-M., J.R.M.-R., J.A.G.-C. and C.E.E.-G.; supervision, E.D.B.-C. and C.E.E.-G.; project administration, C.E.E.-G.; funding acquisition, C.E.E.-G. All authors have read and agreed to the published version of the manuscript.

**Funding:** SECIHTI (formerly CONAHCYT) by means of a Project CF-2023-G-635 approved in the call "Frontier Science" 2023.

**Institutional Review Board Statement:** Not applicable.

**Informed Consent Statement:** Not applicable.

**Data Availability Statement:** All data generated or analyzed during this study are included in this published article.

**Acknowledgments:** The authors acknowledge SECIHTI (formerly CONAHCYT) for supporting a JEC-A PhD fellowship in the program Becas Nacionales de Posgrado, and the support derived from the project approved in 2023 (Frontier Science) that is related to this work. Graphical abstract and Figure 1 were created with BioRender.com.

**Conflicts of Interest:** The authors declare no conflicts of interest.

## References

1. Secretary-General, U.N. *Population, Food Security, Nutrition and Sustainable Development: Report of the Secretary-General*; United Nations: New York, NY, USA, 2021.
2. Sadraei, R.; Biancone, P.; Lanzalonga, F.; Jafari-Sadeghi, V.; Chmet, F. How to Increase Sustainable Production in the Food Sector? Mapping Industrial and Business Strategies and Providing Future Research Agenda. *Bus. Strategy Environ.* **2023**, *32*, 2209–2228. [CrossRef]
3. El-Saadony, M.T.; Saad, A.M.; El-Wafai, N.A.; Abou-Aly, H.E.; Salem, H.M.; Soliman, S.M.; El-Mageed, T.A.A.; Elrys, A.S.; Selim, S.; El-Hack, M.E.A.; et al. Hazardous Wastes and Management Strategies of Landfill Leachates: A Comprehensive Review. *Environ. Technol. Innov.* **2023**, *31*, 103150. [CrossRef]
4. Kumar, A.; Singh, E.; Mishra, R.; Lo, S.L.; Kumar, S. Global Trends in Municipal Solid Waste Treatment Technologies through the Lens of Sustainable Energy Development Opportunity. *Energy* **2023**, *275*, 127471. [CrossRef]
5. Yang, J.; Zhao, Y.; Li, M.; Du, M.; Li, X.; Li, Y. A Review of a Class of Emerging Contaminants: The Classification, Distribution, Intensity of Consumption, Synthesis Routes, Environmental Effects and Expectation of Pollution Abatement to Organophosphate Flame Retardants (Opfrs). *Int. J. Mol. Sci.* **2019**, *20*, 2874. [CrossRef]
6. Vaccari, M.; Tudor, T.; Vinti, G. Characteristics of Leachate from Landfills and Dumpsites in Asia, Africa and Latin America: An Overview. *Waste Manag.* **2019**, *95*, 416–431. [CrossRef]

7. Liu, Z.; de Souza, T.S.P.; Holland, B.; Dunshea, F.; Barrow, C.; Suleria, H.A.R. Valorization of Food Waste to Produce Value-Added Products Based on Its Bioactive Compounds. *Processes* **2023**, *11*, 840. [CrossRef]
8. Mahongnao, S.; Sharma, P.; Nanda, S. Conversion of Waste Materials into Different By-Products of Economic Value. In *Waste Management and Resource Recycling in the Developing World*; Elsevier: Amsterdam, The Netherlands, 2023; pp. 665–699.
9. Varshney, S.; Gupta, A. Forest Industrial Biomass Residue-Mediated Green Synthesized Multifunctional Copper Oxide Nanoparticles for Efficient Wastewater Treatment and Biomedical Applications. *J. Clean. Prod.* **2024**, *434*, 140109. [CrossRef]
10. Osman, A.I.; Zhang, Y.; Farghali, M.; Rashwan, A.K.; Eltaweil, A.S.; El-Monaem, E.M.A.; Mohamed, I.M.A.; Badr, M.M.; Ihara, I.; Rooney, D.W.; et al. Synthesis of Green Nanoparticles for Energy, Biomedical, Environmental, Agricultural, and Food Applications: A Review. *Environ. Chem. Lett.* **2024**, *22*, 841–887. [CrossRef]
11. Sharma, R.; Lata, S.; Garg, R. Valorisation of Agricultural Waste and Their Role in Green Synthesis of Value-Added Nanoparticles. *Environ. Technol. Rev.* **2024**, *13*, 40–59. [CrossRef]
12. FAO. *Citrus Fruit Statistical Compendium 2020*; Food and Agriculture Organization of the United Nations: Rome, Italy, 2021; pp. 1–48.
13. Uthman, A.; Garba, Y. Citrus Mineral Nutrition and Health Benefits: A Review. In *Citrus Research-Horticultural and Human Health Aspects*; IntechOpen: London, UK, 2023.
14. Dongre, P.; Doifode, C.; Choudhary, S.; Sharma, N. Botanical Description, Chemical Composition, Traditional Uses and Pharmacology of *Citrus sinensis*: An Updated Review. *Pharmacol. Res.-Mod. Chin. Med.* **2023**, *8*, 100272. [CrossRef]
15. Minami, G.S.; Lumbantoruan, E.C.; Puteri; Nuraini, R.; Harianto, J.C.; Fahrurroji, A. The Potential of Sweet Orange (*Citrus sinensis*) in Cardiovascular Health: A Literature Review. *J. Kedokt. Dan. Kesehat. Indones.* **2023**, *14*, 82–94. [CrossRef]
16. Bocker, R.; Silva, E.K. Pulsed Electric Field Technology as a Promising Pre-Treatment for Enhancing Orange Agro-Industrial Waste Biorefinery. *RSC Adv.* **2024**, *14*, 2116–2133. [CrossRef]
17. Singh, B.; Singh, J.P.; Kaur, A.; Singh, N. Phenolic Composition, Antioxidant Potential and Health Benefits of Citrus Peel. *Food Res. Int.* **2020**, *132*, 109114. [CrossRef]
18. Ashraf, H.; Iahtisham-Ul-Haq; Butt, M.S.; Nayik, G.A.; Ramniwas, S.; Damto, T.; Alharbi, S.A.; Ansari, M.J. Phytochemical and Antioxidant Profile of Citrus Peel Extracts in Relation to Different Extraction Parameters. *Int. J. Food Prop.* **2024**, *27*, 286–299. [CrossRef]
19. Bekheet, M.A.; Riyad, Y.M.; Hosny, M.H.; El-Ghafar, A.; Mohamed, M. Bioactive Compounds and Antioxidant Activity of Some Fruit and Vegetable Wastes. *Egypt. J. Chem.* **2024**, *67*, 157–166. [CrossRef]
20. Yohannes, R.; Geremew, T.; Tafese, T.; Endale, M. Antibacterial and Antioxidant Activity of Compounds from *Citrus sinensis* L. Peels and in Silico Molecular Docking Study. *Int. J. Second. Metab.* **2023**, *10*, 437–458. [CrossRef]
21. Viñas-Ospino, A.; Jesus, A.R.; Paiva, A.; Esteve, M.J.; Frígola, A.; Blesa, J.; López-Malo, D. Comparison of Green Solvents for the Revalorization of Orange By-Products: Carotenoid Extraction and in vitro Antioxidant Activity. *Food Chem.* **2024**, *442*, 138530. [CrossRef]
22. Wang, Z.; Mei, X.; Chen, X.; Rao, S.; Ju, T.; Li, J.; Yang, Z. Extraction and Recovery of Bioactive Soluble Phenolic Compounds from Brocade Orange (*Citrus sinensis*) Peels: Effect of Different Extraction Methods Thereon. *LWT* **2023**, *173*, 114337. [CrossRef]
23. Bruno, M.R.; Russo, D.; Cetera, P.; Faraone, I.; Giudice, V.L.; Milella, L.; Todaro, L.; Sinisgalli, C.; Fritsch, C.; Dumarçay, S.; et al. Chemical Analysis and Antioxidant Properties of Orange-Tree (*Citrus sinensis* L.) Biomass Extracts Obtained via Different Extraction Techniques. *Biofuels Bioprod. Biorefining* **2020**, *14*, 509–520. [CrossRef]
24. Farhat, A.; Fabiano-Tixier, A.-S.; Maataoui, M.; Maingonnat, J.-F.; Romdhane, M.; Chemat, F. Microwave Steam Diffusion for Extraction of Essential Oil from Orange Peel: Kinetic Data, Extract's Global Yield and Mechanism. *Food Chem.* **2011**, *125*, 255–261. [CrossRef]
25. Charlton, N.C.; Mastyugin, M.; Török, B.; Török, M. Structural Features of Small Molecule Antioxidants and Strategic Modifications to Improve Potential Bioactivity. *Molecules* **2023**, *28*, 1057. [CrossRef] [PubMed]
26. Brett, A.M.O.; Ghica, M.E. Electrochemical Oxidation of Quercetin. *Electroanalysis* **2003**, *15*, 1745–1750. [CrossRef]
27. Niluxsshun, M.C.D.; Masilamani, K.; Mathiventhan, U. Green Synthesis of Silver Nanoparticles from the Extracts of Fruit Peel of *Citrus tangerina*, *Citrus sinensis*, and *Citrus limon* for Antibacterial Activities. *Bioinorg. Chem. Appl.* **2021**, *2021*, 6695734. [CrossRef] [PubMed]
28. Sahar, T.; Munir, H.; Zia, Z.; Nageen; Rafiq, N.; Shafiq, N.; Aleem, S.; Aslam, S. Ecofriendly Green Synthesis of Iron Oxide Nanoparticles Using *Citrus sinensis*. *Front. Chem. Sci.* **2020**, *1*, 21–28. [CrossRef]
29. Gao, Y.; Xu, D.; Ren, D.; Zeng, K.; Wu, X. Green Synthesis of Zinc Oxide Nanoparticles Using *Citrus sinensis* Peel Extract and Application to Strawberry Preservation: A Comparison Study. *LWT* **2020**, *126*, 109297. [CrossRef]
30. Salem, S.S.; Badawy, M.S.E.M.; Al-Askar, A.A.; Arishi, A.A.; Elkady, F.M.; Hashem, A.H. Green Biosynthesis of Selenium Nanoparticles Using Orange Peel Waste: Characterization, Antibacterial and Antibiofilm Activities against Multidrug-Resistant Bacteria. *Life* **2022**, *12*, 893. [CrossRef]

31. Rai, M.; Ingle, A.P.; Pandit, R.; Paralikar, P.; Shende, S.; Gupta, I.; Biswas, J.K.; da Silva, S.S. Copper and Copper Nanoparticles: Role in Management of Insect-Pests and Pathogenic Microbes. *Nanotechnol. Rev.* **2018**, *7*, 303–315. [CrossRef]
32. Dakal, T.C.; Kumar, A.; Majumdar, R.S.; Yadav, V. Mechanistic Basis of Antimicrobial Actions of Silver Nanoparticles. *Front. Microbiol.* **2016**, *7*, 1831. [CrossRef]
33. Netala, V.R.; Kotakadi, V.S.; Nagam, V.; Bobbu, P.; Ghosh, S.B.; Tartte, V. First Report of Biomimetic Synthesis of Silver Nanoparticles Using Aqueous Callus Extract of Centella Asiatica and Their Antimicrobial Activity. *Appl. Nanosci.* **2015**, *5*, 801–807. [CrossRef]
34. Singh, J.; Kaur, G.; Kaur, P.; Bajaj, R.; Rawat, M. A review on green synthesis and characterization of silver nanoparticles and their applications: A green nanoworld. *World J. Pharm. Pharm. Sci.* **2016**, *5*, 730–762. [CrossRef]
35. Reidy, B.; Haase, A.; Luch, A.; Dawson, K.A.; Lynch, I. Mechanisms of Silver Nanoparticle Release, Transformation and Toxicity: A Critical Review of Current Knowledge and Recommendations for Future Studies and Applications. *Materials* **2013**, *6*, 2295–2350. [CrossRef]
36. Dayem, A.A.; Hossain, M.K.; Lee, S.B.; Kim, K.; Saha, S.K.; Yang, G.M.; Choi, H.Y.; Cho, S.G. The Role of Reactive Oxygen Species (ROS) in the Biological Activities of Metallic Nanoparticles. *Int. J. Mol. Sci.* **2017**, *18*, 120. [CrossRef] [PubMed]
37. Bogdanović, U.; Lazić, V.; Vodnik, V.; Budimir, M.; Marković, Z.; Dimitrijević, S. Copper Nanoparticles with High Antimicrobial Activity. *Mater. Lett.* **2014**, *128*, 75–78. [CrossRef]
38. Crisan, M.C.; Teodora, M.; Lucian, M. Copper Nanoparticles: Synthesis and Characterization, Physiology, Toxicity and Antimicrobial Applications. *Appl. Sci.* **2021**, *12*, 141. [CrossRef]
39. Gudkov, S.V.; Burmistrov, D.E.; Serov, D.A.; Rebezov, M.B.; Semenova, A.A.; Lisitsyn, A.B. Do Iron Oxide Nanoparticles Have Significant Antibacterial Properties? *Antibiotics* **2021**, *10*, 884. [CrossRef]
40. Mandal, A.K.; Katuwal, S.; Tettey, F.; Gupta, A.; Bhattarai, S.; Jaisi, S.; Bhandari, D.P.; Shah, A.K.; Bhattarai, N.; Parajuli, N. Current Research on Zinc Oxide Nanoparticles: Synthesis, Characterization, and Biomedical Applications. *Nanomaterials* **2022**, *12*, 3066. [CrossRef] [PubMed]
41. Khan, I.; Saeed, K.; Khan, I. Nanoparticles: Properties, Applications and Toxicities. *Arab. J. Chem.* **2019**, *12*, 908–931. [CrossRef]
42. Larosi, M.B.; del Val García, J.; Rodríguez, A.R. Laser Synthesis of Nanomaterials. *Nanomaterials* **2022**, *12*, 2903. [CrossRef]
43. Gorrasi, G.; Sorrentino, A. Mechanical Milling as a Technology to Produce Structural and Functional Bio-Nanocomposites. *Green. Chem.* **2015**, *17*, 2610–2625. [CrossRef]
44. Rajput, N. Methods of Preparation of Nanoparticles–A Review. *IJAET* **2015**, *7*, 1806–1811.
45. Rana, A.; Yadav, K.; Jagadevan, S. A Comprehensive Review on Green Synthesis of Nature-Inspired Metal Nanoparticles: Mechanism, Application and Toxicity. *J. Clean. Prod.* **2020**, *272*, 122880. [CrossRef]
46. Singh, J.; Dutta, T.; Kim, K.H.; Rawat, M.; Samddar, P.; Kumar, P. "Green" Synthesis of Metals and Their Oxide Nanoparticles: Applications for Environmental Remediation. *J. Nanobiotechnol.* **2018**, *16*, 84. [CrossRef] [PubMed]
47. M'hiri, N.; Ioannou, I.; Boudhrioua, N.M.; Ghoul, M. Effect of Different Operating Conditions on the Extraction of Phenolic Compounds in Orange Peel. *Food Bioprod. Process.* **2015**, *96*, 161–170. [CrossRef]
48. Cavaleri, J.S.; Rankin, D.I.; Harbeck, J.K.; Sautter, L.R.; McCarter, S.Y.; Sharp, S.E. *Manual of Antimicrobial Susceptibility Testing*; American Society for Microbiology: Seattle, WA, USA, 2005.
49. Andrews, J.M. Determination of Minimum Inhibitory Concentrations. *J. Antimicrob. Chemother.* **2001**, *48*, 5–16. [CrossRef]
50. Abdelghffar, E.A.; El-Nashar, H.A.S.; Al-Mohammadi, A.G.A.; Eldahshan, O.A. Orange Fruit (*Citrus sinensis*) Peel Extract Attenuates Chemotherapy-Induced Toxicity in Male Rats. *Food Funct.* **2021**, *12*, 9443–9455. [CrossRef]
51. Chen, Z.T.; Chu, H.L.; Chyau, C.C.; Chu, C.C.; Duh, P. Der Protective Effects of Sweet Orange (*Citrus sinensis*) Peel and Their Bioactive Compounds on Oxidative Stress. *Food Chem.* **2012**, *135*, 2119–2127. [CrossRef]
52. Elsheikh, M.M.; Agamy, N.F.; Elnouby, M.S.; Ismail, H.M. Green Synthesis of Silver Nanoparticles Using Various Food Wastes. *FPMPEB* **2024**, *1*, 13–17. [CrossRef]
53. Jahan, I.; Erci, F.; Isildak, I. Facile Microwave-Mediated Green Synthesis of Non-Toxic Copper Nanoparticles Using *Citrus sinensis* Aqueous Fruit Extract and Their Antibacterial Potentials. *J. Drug Deliv. Sci. Technol.* **2021**, *61*, 102172. [CrossRef]
54. Faruruwa, M.D.; Adamu, H.; Adeyemi, M.M.; Tomori, W.B. Green Synthesis of Iron (III) Oxide ($Fe_3O_4$) Nanoparticles Using *Citrus sinensis* Peel Extract for the Removal of Ciprofloxacin in Water. *J. Appl. Sci. Environ. Manag.* **2024**, *28*, 823–839. [CrossRef]
55. Thakral, F.; Tuli, H.S.; Gupta, S.; Joshi, H.; Ashgar, S.S.; Faidah, H.; Bantun, F.; Slama, P.; Haque, S. Synergistic Anti-Bacterial Effects of Green Synthesized Zinc Oxide Nanoparticles with Levofloxacin. *J. King Saud. Univ. Sci.* **2023**, *35*, 102905. [CrossRef]
56. Duarte, J.; Cruz-Lopes, L.; Dulyanska, Y.; Domingos, I.; Ferreira, J.; Ferreira, J.; Lemos, L.T.D.; Esteves, B. Orange peel liquefaction monitored by ftir. *J. Int. Sci. Publ.* **2017**, *5*, 309–313.
57. Yaradoddi, J.S.; Banapurmath, N.R.; Ganachari, S.V.; Soudagar, M.E.M.; Sajjan, A.M.; Kamat, S.; Mujtaba, M.A.; Shettar, A.S.; Anqi, A.E.; Safaei, M.R.; et al. Bio-Based Material from Fruit Waste of Orange Peel for Industrial Applications. *J. Mater. Res. Technol.* **2022**, *17*, 3186–3197. [CrossRef]

58. Miranda, R.; Bustos-Martinez, D.; Blanco, C.S.; Villarreal, M.H.G.; Cantú, M.E.R. Pyrolysis of Sweet Orange (*Citrus sinensis*) Dry Peel. *J. Anal. Appl. Pyrolysis* **2009**, *86*, 245–251. [CrossRef]
59. Michael-Igolima, U.; Abbey, S.J.; Ifelebuegu, A.O.; Eyo, E.U. Modified Orange Peel Waste as a Sustainable Material for Adsorption of Contaminants. *Materials* **2023**, *16*, 1092. [CrossRef]
60. Sang, J.; Li, L.; Wen, J.; Gu, Q.; Wu, J.; Yu, Y.; Xu, Y.; Fu, M.; Lin, X. Evaluation of the Structural, Physicochemical and Functional Properties of Dietary Fiber Extracted from Newhall Navel Orange by-Products. *Foods* **2021**, *10*, 2772. [CrossRef]
61. Noman, M.; Shahid, M.; Ahmed, T.; Niazi, M.B.K.; Hussain, S.; Song, F.; Manzoor, I. Use of Biogenic Copper Nanoparticles Synthesized from a Native Escherichia Sp. as Photocatalysts for Azo Dye Degradation and Treatment of Textile Effluents. *Environ. Pollut.* **2020**, *257*, 113514. [CrossRef]
62. Toprakçı, İ.; Balci-Torun, F.; Deniz, N.G.; Ortaboy, S.; Torun, M.; Şahin, S. Recovery of Citrus Volatile Substances from Orange Juice Waste: Characterization with GC-MS, FTIR, 1H- and 13C-NMR Spectroscopies. *Phytochem. Lett.* **2023**, *57*, 177–184. [CrossRef]
63. Tarhan, İ.; Çelikten, Ş.; Kestek, H.M.; Çelik, B.; Öner, M.; Kenar, A.; Kara, H. Development of a New and Rapid FTIR Method Using Chemometric Modeling Techniques for the Determination of Lavandin Adulteration in Lavender Essential Oil. *Vib. Spectrosc.* **2023**, *127*, 103559. [CrossRef]
64. Figueira, O.; Pereira, V.; Castilho, P.C. A Two-Step Approach to Orange Peel Waste Valorization: Consecutive Extraction of Pectin and Hesperidin. *Foods* **2023**, *12*, 3834. [CrossRef]
65. Muthuselvi, C.; Sabapathy, S.; Ravikumar, B.; Athimoolam, S.; Srinivasan, N.; Venkatrama, R. Synthesis, Vibrational and Optical Studies of Indeno Quinoxaline Pyrrolo Thiazole Derivative Crystal. *Asian J. Appl. Sci.* **2018**, *11*, 140–150. [CrossRef]
66. Giechaskiel, B.; Clairotte, M. Fourier Transform Infrared (Ftir) Spectroscopy for Measurements of Vehicle Exhaust Emissions: A Review. *Appl. Sci.* **2021**, *11*, 7416. [CrossRef]
67. Niu, Y.; Gao, Y.; Xiao, Z.; Mao, C.; Wang, H.; Geng, Y.; Ye, Y.; Kou, X. Preparation and Characterisation of Linalool Oil-in-Water Starch-Based Pickering Emulsions and the Effects of the Addition of Cellulose Nanocrystals on Their Stability. *Int. J. Biol. Macromol.* **2023**, *247*, 125732. [CrossRef] [PubMed]
68. Corbu, V.M.; Dumbravă, A.Ş.; Marinescu, L.; Motelica, L.; Chircov, C.; Surdu, A.V.; Gheorghe-Barbu, I.; Pecete, I.; Balotescu, I.; Popa, M.; et al. Alternative Mitigating Solutions Based on Inorganic Nanoparticles for the Preservation of Cultural Heritage. *Front. Mater.* **2023**, *10*, 1272869. [CrossRef]
69. Munir, I.; Yesiloz, G. Novel Size-Tunable and Straightforward Ultra-Small Nanoparticle Synthesis in a Varying Concentration Range of Glycerol as a Green Reducing Solvent. *ACS Omega* **2023**, *8*, 28456–28466. [CrossRef]
70. Brumbaugh, A.D.; Cohen, K.A.; Angelo, S.K.S. Ultrasmall Copper Nanoparticles Synthesized with a Plant Tea Reducing Agent. *ACS Sustain. Chem. Eng.* **2014**, *2*, 1933–1939. [CrossRef]
71. Ebrahiminezhad, A.; Taghizadeh, S.; Ghasemi, Y.; Berenjian, A. Green Synthesized Nanoclusters of Ultra-Small Zero Valent Iron Nanoparticles as a Novel Dye Removing Material. *Sci. Total Environ.* **2018**, *621*, 1527–1532. [CrossRef]
72. Zarate-Escobedo, J.; Zavaleta-Mancera, H.A.; Soto-Hernández, R.M.; Pérez-Rodríguez, P.; Vilchis-Nestor, A.R.; Silva-Rojas, H.V.; Trejo-Téllez, L.I. Long-Lasting Silver Nanoparticles Synthesized with Tagetes Erecta and Their Antibacterial Activity against Erwinia Amylovora, a Serious Rosaceous Pathogen. *Plants* **2024**, *13*, 981. [CrossRef]
73. Anwar, S.J.; Yusoff, H.M.; Bhat, I.U.H.; Ern, L.K. Remediation of Dye-Contaminated Water Using Brown Algae Seaweed Supported Copper Nanoparticles. *Arab. J. Sci. Eng.* **2024**, *49*, 475–496. [CrossRef]
74. Alamu, G.A.; Ayanlola, P.S.; Babalola, K.K.; Adedokun, O.; Sanusi, Y.K.; Fajinmi, G.R. Green Synthesis and Characterizations of Magnetic Iron Oxide Nanoparticles Using Moringa Oleifera Extract for Improved Performance in Dye-Sensitized Solar Cell. *Chem. Phys. Impact* **2024**, *8*, 100542. [CrossRef]
75. Kadir, N.H.A.; Murugan, N.; Khan, A.A.; Sandrasegaran, A.; Khan, A.U.; Alam, M. Evaluation of the Cytotoxicity, Antioxidant Activity, and Molecular Docking of Biogenic Zinc Oxide Nanoparticles Derived from Pumpkin Seeds. *Microsc. Res. Tech.* **2024**, *87*, 602–615. [CrossRef]
76. Din, M.I.; Arshad, F.; Hussain, Z.; Mukhtar, M. Green Adeptness in the Synthesis and Stabilization of Copper Nanoparticles: Catalytic, Antibacterial, Cytotoxicity, and Antioxidant Activities. *Nanoscale Res. Lett.* **2017**, *12*, 638. [CrossRef] [PubMed]
77. Fievet, F.; Ammar-Merah, S.; Brayner, R.; Chau, F.; Giraud, M.; Mammeri, F.; Peron, J.; Piquemal, J.Y.; Sicard, L.; Viau, G. The polyol process: A unique method for easy access to metal nanoparticles with tailored sizes, shapes and compositions. *Chem. Soc. Rev.* **2018**, *47*, 5187–5233. [CrossRef]
78. Naaz, R.; Siddiqui, V.U.; Qadir, S.U.; Siddiqi, W.A. Green Synthesis of Silver Nanoparticles Using Syngonium Podophyllum Leaf Extract and Its Antibacterial Activity. In Proceedings of the Materials Today: Proceedings; Elsevier Ltd.: Oxford, UK, 2021; pp. 2352–2358.
79. Korkmaz, N.; Ceylan, Y.; Hamid, A.; Karadağ, A.; Bülbül, A.S.; Aftab, M.N.; Çevik, Ö.; Şen, F. Biogenic Silver Nanoparticles Synthesized via Mimusops Elengi Fruit Extract, a Study on Antibiofilm, Antibacterial, and Anticancer Activities. *J. Drug Deliv. Sci. Technol.* **2020**, *59*, 101864. [CrossRef]

80. Rashnaei, N.; Siadat, S.D.; Sepahi, A.A.; Mirzaee, M.; Bahramali, G.; Joshaghani, A.A. Green Synthesized Silver Nanoparticles Using Anise (*Pimpinella anisum* L.) Have Antibacterial Effects. *Vaccine Res.* **2020**, *7*, 17–24. [CrossRef]
81. Yousef, A.; Abu-Elghait, M.; Barghoth, M.G.; Elazzazy, A.M.; Desouky, S.E. Fighting Multidrug-Resistant Enterococcus Faecalis via Interfering with Virulence Factors Using Green Synthesized Nanoparticles. *Microb. Pathog.* **2022**, *173*, 105842. [CrossRef] [PubMed]
82. Zangeneh, M.M.; Ghaneialvar, H.; Akbaribazm, M.; Ghanimatdan, M.; Abbasi, N.; Goorani, S.; Pirabbasi, E.; Zangeneh, A. Novel Synthesis of Falcaria Vulgaris Leaf Extract Conjugated Copper Nanoparticles with Potent Cytotoxicity, Antioxidant, Antifungal, Antibacterial, and Cutaneous Wound Healing Activities under in Vitro and in Vivo Condition. *J. Photochem. Photobiol. B* **2019**, *197*, 111556. [CrossRef]
83. Ismail, N.A.; Shameli, K.; Wong, M.M.T.; Teow, S.Y.; Chew, J.; Sukri, S.N.A.M. Antibacterial and Cytotoxic Effect of Honey Mediated Copper Nanoparticles Synthesized Using Ultrasonic Assistance. *Mater. Sci. Eng. C* **2019**, *104*, 109899. [CrossRef]
84. Vinothini, P.; Malaikozhundan, B.; Krishnamoorthi, R.; Senthamarai, M.D.; Shanthi, D. Potential Inhibition of Biofilm Forming Bacteria and Fungi and DPPH Free Radicals Using Tamarindus Indica Fruit Extract Assisted Iron Oxide Nanoparticle. *Inorg. Chem. Commun.* **2023**, *156*, 111206. [CrossRef]
85. Alavi, M.; Karimi, N. Ultrasound Assisted-Phytofabricated $Fe_3O_4$ NPs with Antioxidant Properties and Antibacterial Effects on Growth, Biofilm Formation, and Spreading Ability of Multidrug Resistant Bacteria. *Artif. Cells Nanomed. Biotechnol.* **2019**, *47*, 2405–2423. [CrossRef]
86. Ifeanyichukwu, U.L.; Fayemi, O.E.; Ateba, C.N. Green Synthesis of Zinc Oxide Nanoparticles from Pomegranate (*Punica granatum*) Extracts and Characterization of Their Antibacterial Activity. *Molecules* **2020**, *25*, 4521. [CrossRef]
87. El-Kattan, N.; Emam, A.N.; Mansour, A.S.; Ibrahim, M.A.; El-Razik, A.B.A.; Allam, K.A.M.; Riad, N.Y.; Ibrahim, S.A. Curcumin Assisted Green Synthesis of Silver and Zinc Oxide Nanostructures and Their Antibacterial Activity against Some Clinical Pathogenic Multi-Drug Resistant Bacteria. *RSC Adv.* **2022**, *12*, 18022–18038. [CrossRef] [PubMed]


**Disclaimer/Publisher's Note:** The statements, opinions and data contained in all publications are solely those of the individual author(s) and contributor(s) and not of MDPI and/or the editor(s). MDPI and/or the editor(s) disclaim responsibility for any injury to people or property resulting from any ideas, methods, instructions or products referred to in the content.